Inorganic Chemistry

Communication

pubs.acs.org/IC

Enantioselective Inclusion of Alcohols by Solvent-Controlled Assembled Flexible Metal−Organic Frameworks

Lang Lin, Rongmin Yu,* Xiao-Yuan Wu, Wen-Bin Yang, Jian Zhang, Xiang-Guang Guo, Zu-Jin Lin, and Can-Zhong Lu*

State Key Laboratory of Structural Chemistry, Fujian Institute of Research on the Structure of Matter, Chinese Academy of Sciences, Fuzhou, Fujian 35002, China

Supporting Information

ABSTRACT: Through judicious choice of the ligands and patient regulation of the solvent conditions, three unique chiral coordination polymeric isomers have been synthesized. Their structures, gas adsorption, and structural interconversion have been studied. One of the isomers displays dynamic behavior, and its use in the enantioselective separation of chiral alcohols has also been reported.

Chiral metal−organic frameworks (MOFs), which can be afforded by self-assembly reactions of chiral organic linkers and metal ions, usually exhibit intriguing homochiral structures as well as fascinating potential applications.[1] To date, considerable interest has been focused on the use of chiral MOFs for enantioseparation in virtue of their stable chiral architectures, controllable open cavities and tunable intermolecular interactions.[2] Recent breakthroughs of their applications in the area of chromatographic and membrane-based separation demonstrate their potential applications as a new generation of chiral resolving agents.[3] However, relative researches are still very scarce.

A key point to designing chiral MOFs with porous frameworks and enantioseparation properties is to choose the proper chiral building blocks. However, the design and preparation remain challenging mainly because of the limited chiral source and tedious synthetic process of the ligands.[4] Hence, readily available chiral polydentate ligands are highly desired. Amino acids and their derivatives are attractive because of their inherent chirality, inexpensive price, multiple coordination modes, and modifiable structures. In addition, amino acid based MOFs are rich in donors and acceptors for hydrogen-bonding interactions that are of importance for effective enantioselective recognition.[5]

Amino acid based chiral MOFs are reported to be increasing each year,[6] but most of them are of condensed packing structures without accessible pores or channels, mainly resulting from the backbone flexibility of the amino acids.[7] To construct open porous architectures, rigid ligands are usually adopted to strengthen the frameworks and pillar cavities.[8] Moreover, synthetic conditions are also needed to regulate patiently. Reaction media are extremely significant because they not only make a great impact on the reactants' solubility and polarity but also act as templates to induce structural formation and crystallization.

In this study, rare examples of amino acid based chiral MOFs used for enantioselective adsorption are reported. We employ *N*,*N*′-oxalylbis(alanine) (OBAla) as a flexible enantiopure ligand,[9] along with 4,4′-methylenedi-3,5-dimethylpyrazole (H_2mbdpz) as a conformationally flexible auxiliary ligand, to construct three homochiral coordination polymeric isomers under different solvent conditions, formulated as Cu_2(L-OBAla)(H_2mbdpz)$_2$ (**1**), α-Cu_2(L-OBAla)(H_2mbdpz) (**2**), and β-Cu_2(L-OBAla)(H_2mbdpz)⊃guest (**3**⊃**guest**) (Scheme 1). The significant role of the solvent in framework formation is further demonstrated by solvent-induced interconversion of compounds **2** and **3**. Moreover, compound **3** undergoes a reversible structural transformation during guest exchange and exhibits enantioselective inclusion of aromatic alcohols.

Scheme 1. Structures of the Ligands and Subunit[a]

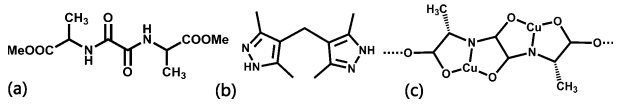

[a](a) OBAla ligand; (b) H_2mbdpz ligand; (c) Cu_2(L-OBAla) subunits.

Hydrothermal reactions of $Cu(NO_3)_2$, OBAla, and H_2mbdpz in a molar ratio of 2:1:1 at 100 °C for 3 days afford light-green sheet-like crystals of compound **1**. When water is replaced with a mixture of EtOH (or CH_3CN, DMA)/H_2O (1:3, v/v), blue spindle-shaped crystals of compound **2** are obtained. Light-green polyhedral crystals of compound **3** are the main product in the mixture of water and 2-butanol [or other alcohols such as isopropyl alcohol, 2-pentanol, 2-hexanol, 2-heptanol, 1-phenethyl alcohol (1-PEA), 1-phenyl-1-propanol (1-PPP)]. Compounds **1**, **2**, and **3**⊃**guest** can be easily distinguished by their shape and color (Figure S1 in the Supporting Information, SI). All compounds are insoluble in common organic solvents.

Single-crystal X-ray crystallographic studies reveal that all of the compounds contain planar Cu_2(OBAla) subunits, which are similar to our previous report (Scheme 1c).[9b] In this subunit, a −NH−CO−CO−NH− (*N*,*N*′-disubstituted oxamide) core and two terminal carboxyl groups chelate two Cu atoms in a bis-tridentate manner, forming four five-membered rings. Each Cu atom is five-coordinated in a distorted square-pyramidal geometry. Compound **1** crystallizes in the triclinic space group *P*1. The adjacent Cu_2(OBAla) subunits are linked to each other via the four H_2mbdpz ligands to form a 1D loop chain running along the *b* axis (Figures S22 and S23 in the SI).

Received: February 25, 2014
Published: April 30, 2014

dx.doi.org/10.1021/ic500436g | *Inorg. Chem.* 2014, 53, 4794−4796

Compounds **2** and **3⊃2-BuOH** have identical coordination modes and crystallize in the chiral space groups $P4_12_12$ and $P4_32_12$, respectively. The binuclear copper subunits are connected to each other through bonds contributed by pyrazole N atoms of H_2mbdpz ligands in the basal plane, as well as apical Cu−O bonds contributed by carboxyl O atoms of L-OBAla ligands from other Cu_2(OBAla) subunits. Therefore, if Cu_2(OBAla) is simplified as six-connected nodes, **2** and **3⊃2-BuOH** display 3D noninterpenetrating frameworks with *lcy* topology (Figure S24 in the SI). Along the *c* axis, there are two types of right-handed helical chains in both compounds: a 4_1 helix composed of Cu_2(OBAla) subunits and a 2_1 helix constructed by the copper subunits and H_2mbdpz ligands (Figure S26 in the SI). The 2_1 helix generates a rectangular channel with a small size of 3.2 × 3.2 Å in compound **2**, whose cavity is seriously blocked by four methyl groups pointing to the center of the channel (Figure 1b). However, with methyl groups located on the wall of the tubular channels, compound **3⊃2-BuOH** has a channel with a square cross section of approximately 5.7 × 8.1 $Å^2$ (Figure 1d). *PLATON* analysis shows that the void space is 24.1% of the total volume in **2**. The porosity rises to 34.6% in **3⊃2-BuOH** if guest molecules are not included, which is 43% higher than that of **2** (Figure 1e,f).

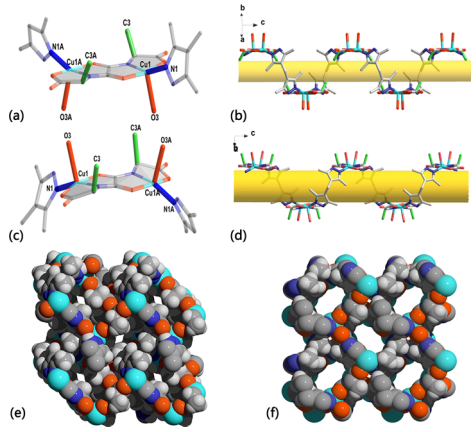

Figure 1. (a) Coordination environment for L-OBAla in **2**. (b) 1D helix chains in **2**. (c) Coordination environment for L-OBAla in **3**. (d) 1D helix chains in **3**. (e) Space-filling models of **2**. (f) Space-filling models of **3** viewed along the *c* axis (solvent molecules have been omitted for clarity).

Close observation reveals that the difference in the conformation of pyrazoles causes dissimilar structural features of compounds **2** and **3⊃2-BuOH**. Consequently, the C3 and O3 atoms locate on the opposite side of the Cu_2(OBAla) plane in compound **2**, while the two atoms reside on the same side in **3⊃2-BuOH** (Figure 1a,c). If guests were not considered, the two compounds would be classified as "conformational isomers".[10]

The powder X-ray diffraction (PXRD) patterns of all compounds are in good agreement with the simulated ones, suggesting the purity of the products (Figure S9 in the SI). The circular dichroism (CD) curves of the three compounds, produced from L- or D-OBAla, are mirror images of each other, which suggests their enantiomeric nature (Figure S2 in the SI). Notably, the different CD curves of isomers **2** and **3** allow us to discern them by CD spectra.

The guest molecules, 2-butanol, in compound **3⊃2-BuOH** are disordered in structure. However, the high boiling guest molecules in compounds **3⊃1-PEA** and **3⊃1-PPP** have been clearly determined by single-crystal X-ray diffraction (Figure S27 in the SI). Compounds **3⊃1-PEA** and **3⊃1-PPP** crystallize in the space group $P2_12_12$ with skeletons that are nearly identical with that of **3⊃2-BuOH**. Each asymmetric unit involves one guest molecule. According to the crystallography data that we collected, the chiral framework of L-**3** attracts (*R*)-1-PEA and (*S*)-1-PPP, while D-**3** adsorbs (*S*)-1-PEA and (*R*)-1-PPP.

Because the solvent is the only variable in the reaction conditions, some empirical trends are found according to the relationship between the solvent and final products (Table S12 in the SI). Polar solvents prompt the assembly of **1** and **2**, while lower polar solvents result in the formation of **3**. Small solvent molecules lead to the construction of dense packing structures of **2**; however, molecules that are larger than C5 can be served as templates to generate the large pores of **3**.

Not only in the forming stage do the solvents have an influence on the thermal postprocessing of formed crystals. It has been observed that the blue crystals of **2** can convert to green powders of **3⊃1-PEA** in the H_2O/1-PEA mixture for 2 days under hydrothermal conditions. Similarly, **3** can also convert to **2** by heating in the H_2O/EtOH mixtures (Figure 2a). The PXRD patterns and CD spectra before and after solvothermal reactions further demonstrate the occurrence of interconversion (Figures S3, S4, S14, and S15 in the SI). Because the compound experiences a process of bond breaking and regeneration, we consider that interconversion is not through a single crystal-to-single crystal transformation but via a decomposition and reconstruction mechanism.

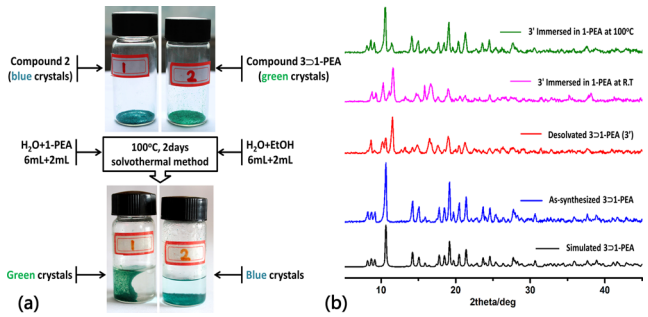

Figure 2. (a) Photographs of the interconversion process of **2** and **3⊃1-PEA**. (b) PXRD patterns for as-synthesized **3⊃1-PEA**, desolvated **3⊃1-PEA** (**3′**), and **3′** immersed in 1-PEA at room temperature and 100 °C for 3 days.

To investigate the crystal stability upon removal of the solvents, thermogravimetric analyses (TGA) and PXRD experiments at variable temperatures are carried out. TGA show that the frameworks of compounds **1**−**3** are stable up to 240 °C. Before framework collapse, compound **3⊃guest** loses one solvent molecule consistent with the formula (Figures S5−S7 in the SI). Notably, when heating at 120 °C, the PXRD pattern of desolvated **3⊃2-BuOH** is distinct from the original pattern. Meanwhile, the crystals become opaque and are unsuitable for single-crystal X-ray diffraction. Removal of the high-boiling-point solvent in **3⊃1-PEA**, **3⊃1-PPP**, or **3⊃2-PenOH** by solvent exchange with methanol also leads to different PXRD patterns, which are close to that of desolvated **3⊃2-BuOH** (Figures S11 and S12 in the SI). These phenomena reveal that no matter which guests are included, removing guests from **3** will generate a desolvated framework of **3′**.

Furthermore, gas adsorption experiments confirm the structural transformation by the detection of porosity. Activated by heating at 120 °C under vacuum, compound **2** exhibits a type I

dx.doi.org/10.1021/ic500436g | *Inorg. Chem.* 2014, 53, 4794−4796

behavior with a moderate H_2 uptake of 111 cm^3 g^{-1} at 760 mmHg, while desolvated **3⊃2-BuOH** adsorbed none of the three gas probes, including H_2, N_2, and CO_2 (Figure S16 in the SI). The loss of the adsorption capacity of **3** can be attributed to the remarkable shrinking of the pore size during desolvation. Hence, the guest molecules have a profound effect on sustaining and stabilizing the open frameworks.

Interestingly, the guests can infiltrate the framework of **3′** and regenerate **3⊃guest**. This process is clearly verified by the PXRD patterns before and after readsorption. Take **3⊃1-PEA** for example (Figure 2b). The strongest peak moves from 10.6° to 11.5° upon loss of guests, and then it returns to 10.6° after **3′** is immersed in 1-PEA for 3 days at 80 °C, following with the emergence of three characteristic peaks of **3⊃1-PEA** at 2θ = 8.19°, 8.70°, and 9.13°. 1-PPP can also be readsorbed by compound **3′** (Figure S13 in the SI). However, the regeneration process cannot take place at room temperature.

The reversible and dynamic transition of compound **3** prompts us to explore its resolution application on small chiral alcohols, such as 1-PEA, 1-PPP, and 1-(2-naphthyl)ethanol (NPE). L-**3** can enantioselectively include 1-PEA (43.4% ee, in favor of the *R* isomer) and 1-PPP (36.0% ee, in favor of the *S* isomer). The desorbed guests from D-**3** favor the opposite isomers, which agree with the crystal structures described above (Table S13 and Figures S17−S20 in the SI). However, owing to the size effect, the ee values for desorbed NPE are very low. Moreover, desolvated **3′** is able to resolvate and be tested in the next cycle, but the ee values decrease to 34.4% (for 1-PEA) and 26.0% (for 1-PPP), which may be caused by certain loss of crystallinity during solvent exchange and framework transformation (Figure S21 in the SI).

The enantioselectivity can be attributed to hydrogen-bonding interactions between O atom (from oxamide) and hydroxyl groups (from 1-PEA or 1-PPP), which make the guest molecules orderly dock in the channels (Figure 3). The O···O distances of

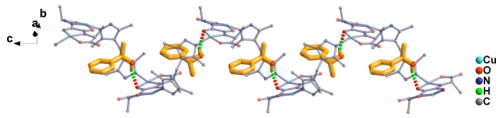

Figure 3. Hydrogen bonds between 1-PEA guests (yellow molecules) and the 1D channel in **3⊃1-PEA** (H atoms have been omitted for clarity except hydroxy H).

O−H···O hydrogen bonds are in the range of 2.9802−3.1348 Å, but the overall affinity of **3** toward alcohol is not strong enough for complete resolution of racemates, resulting in a moderate recognition capability.

The studies in the application of chiral MOFs for chiral aromatic alcohol resolution are extremely rare because large pores are required for aromatic alcohols to accommodate. The enantioselective capability of compound **3** for 1-PEA is lower than that of M′MOF-3−7[4a,b] but higher than that of $[Zn_2(bdc)(S\text{-lac})(dmf)]$,[2b] M′MOF-2[4a] and $Cd_2(L\text{-cps})_4(bix)_4$.[4c] This work not only provides valuable clues for the convenient synthesis of porous chiral MOFs but also explores a new way to design chromatographic stationary phase materials using homochiral MOFs containing inexpensive amino acid derivatives.

■ ASSOCIATED CONTENT

Ⓢ Supporting Information

Experimental procedures, detailed characterization, and X-ray crystallographic files in CIF format. This material is available free of charge via the Internet at http://pubs.acs.org.

■ AUTHOR INFORMATION

Corresponding Authors

*E-mail: czlu@fjirsm.ac.cn. Tel: +86-591-83705794. Fax: +86-591-83714946.

*E-mail: rongminyu@fjirsm.ac.cn. Tel: +86-591-83705794. Fax: +86-591-83714946.

Notes

The authors declare no competing financial interest.

■ ACKNOWLEDGMENTS

This work was supported by the 973 Key Program of the MOST (Grants 2010CB933501 and 2012CB821705), the Chinese Academy of Sciences (Grants KJCX2-YW-319 and KJCX2-EW-H01), the National Natural Science Foundation of China (Grants 21373221, 21221001, 91022008, 91122027, and 51172232), and the Natural Science Foundation of Fujian Province (Grants 2011HZ0001-1, 2012J06006, 2006L2005, and 2014J05026).

■ REFERENCES

(1) (a) Yoon, M.; Srirambalaji, R.; Kim, K. *Chem. Rev.* **2012**, *112*, 1196−1231. (b) Wang, C.; Zhang, T.; Lin, W. *Chem. Rev.* **2012**, *112*, 1084−1104. (c) Morris, R. E.; Bu, X. *Nat. Chem.* **2010**, *2*, 353−361.

(2) (a) Liu, Y.; Xuan, W.; Cui, Y. *Adv. Mater.* **2010**, *22*, 4112−4135. (b) Suh, K.; Yutkin, M. P.; Dybtsev, D. N.; Fedin, V. P.; Kim, K. *Chem. Commun.* **2012**, *48*, 513−515.

(3) (a) Nuzhdin, A. L.; Dybtsev, D. N.; Bryliakov, K. P.; Talsi, E. P.; Fedin, V. P. *J. Am. Chem. Soc.* **2007**, *129*, 12958−12959. (b) Zhang, M.; Pu, Z.-J.; Chen, X.-L.; Gong, X.-L.; Zhu, A.-X.; Yuan, L.-M. *Chem. Commun.* **2013**, *49*, 5201−5203. (c) Kang, Z.; Xue, M.; Fan, L.; Ding, J.; Guo, L.; Gao, L.; Qiu, S. *Chem. Commun.* **2013**, *49*, 10569−10571.

(4) (a) Xiang, S. C.; Zhang, Z. J.; Zhao, C. G.; Hong, K. L.; Zhao, X. B.; Ding, D. R.; Xie, M. H.; Wu, C. D.; Das, M. C.; Gill, R.; Thomas, K. M.; Chen, B. L. *Nat. Commun.* **2011**, *2*, 204−210. (b) Das, M. C.; Guo, Q.; He, Y.; Kim, J.; Zhao, C.-G.; Hong, K.; Xiang, S.; Zhang, Z.; Thomas, K. M.; Krishna, R.; Chen, B. *J. Am. Chem. Soc.* **2012**, *134*, 8703−8710. (c) Li, Z.-J.; Yao, J.; Tao, Q.; Jiang, L.; Lu, T.-B. *Inorg. Chem.* **2013**, *52*, 11694−11696.

(5) Vaidhyanathan, R.; Bradshaw, D.; Rebilly, J.-N.; Barrio, J. P.; Gould, J. A.; Berry, N. G.; Rosseinsky, M. J. *Angew. Chem., Int. Ed.* **2006**, *45*, 6495−6499.

(6) (a) Imaz, I.; Rubio-Martinez, M.; An, J.; Sole-Font, I.; Rosi, N. L.; Maspoch, D. *Chem. Commun.* **2011**, *47*, 7287−7302. (b) Chen, L.; Bu, X. *Chem. Mater.* **2006**, *18*, 1857−1860. (c) Rabone, J.; Yue, Y.-F.; Chong, S. Y.; Stylianou, K. C.; Bacsa, J.; Bradshaw, D.; Darling, G. R.; Berry, N. G.; Khimyak, Y. Z.; Ganin, A. Y.; Wiper, P.; Claridge, J. B.; Rosseinsky, M. J. *Science* **2010**, *329*, 1053−1057.

(7) Lee, H.-Y.; Kampf, J. W.; Park, K. S.; Marsh, E. N. G. *Cryst. Growth Des.* **2008**, *8*, 296−303.

(8) Perez Barrio, J.; Rebilly, J. N.; Carter, B.; Bradshaw, D.; Bacsa, J.; Ganin, A. Y.; Park, H.; Trewin, A.; Vaidhyanathan, R.; Cooper, A. I.; Warren, J. E.; Rosseinsky, M. J. *Chem.—Eur. J.* **2008**, *14*, 4521−4532.

(9) (a) Ranganathan, D.; Vaish, N. K.; Chandramouli, G. V. R.; Varghese, B.; Muthukumaran, R. B.; Manoharan, P. T. *J. Am. Chem. Soc.* **1995**, *117*, 1643−1644. (b) Lin, L.; Yu, R.; Yang, W.; Wu, X.-Y.; Lu, C.-Z. *Cryst. Growth Des.* **2012**, *12*, 3304−3311.

(10) Makal, T. A.; Yakovenko, A. A.; Zhou, H.-C. *J. Phys. Chem. Lett.* **2011**, *2*, 1682−1689.